Online Nanoparticle Mass Measurement by Combined Aerosol Particle Mass Analyzer and Differential Mobility Analyzer: Comparison of Theory and Measurements

Anshuman Amit Lall [a]; Xiaofei Ma [a]; Suvajyoti Guha [ab]; George W. Mulholland [ab]; Michael R. Zachariah [ab]

[a] University of Maryland, College Park, Maryland, USA [b] National Institute of Standards and Technology, Gaithersburg, Maryland, USA

First published on: 01 November 2009

PLEASE SCROLL DOWN FOR ARTICLE

Online Nanoparticle Mass Measurement by Combined Aerosol Particle Mass Analyzer and Differential Mobility Analyzer: Comparison of Theory and Measurements

Anshuman Amit Lall,[1] Xiaofei Ma,[1] Suvajyoti Guha,[1,2] George W. Mulholland,[1,2] and Michael R. Zachariah[1,2]

[1]*University of Maryland, College Park, Maryland, USA*
[2]*National Institute of Standards and Technology, Gaithersburg, Maryland, USA*

A combination of a differential mobility analyzer (DMA) and aerosol particle mass analyzer (APM) is used to measure the mass of NIST Standard Reference Materials (SRM®) PSL spheres with 60 and 100 nm nominal diameter, and NIST traceable 300 nm PSL spheres. The calibration PSL spheres were previously characterized by modal diameter and spread in particle size. We used the DMA to separate the particles with modal diameter in a narrow mobility diameter range. The mass of the separated particles is measured using the APM. The measured mass is converted to diameter using a specific density of 1.05. We found that there was good agreement between our measurements and calibration modal diameter. The measured average modal diameters are 59.23 and 101.2 nm for nominal diameters of 60 and 100 nm (calibration modal diameter: 60.39 and 100.7 nm) PSL spheres, respectively. The repeatability uncertainty of these measurements is reported. For 300 nm, the measured diameter was 305.5 nm, which is an agreement with calibration diameter within 1.8%.

The effect of spread in particle size on the APM transfer function is investigated. Two sources of the spread in "mono-dispersed" particle size distributions are discussed: (a) spread due to the triangular DMA transfer function, and (b) spread in the calibration particle size. The APM response function is calculated numerically with parabolic flow through the APM and diffusion broadening. As expected from theory, the calculated APM response function and measured data followed a similar trend with respect to APM voltage. However, the theoretical APM transfer function is narrower than the measured APM response.

INTRODUCTION

An aerosol particle mass analyzer (APM) has recently been used in a number of studies for direct measurement of particle mass (Lall et al. 2008; McMurry et al. 2002; Park et al. 2004; Zhou et al. 2008). The APM classifies particles by balancing the

electrostatic and centrifugal forces (Ehara et al. 1996). The centrifugal force is directly proportional to the particle mass which makes it possible to determine particle mass directly through APM measurements. The method is particularly useful for determining particle mass for non-spherical single or aggregate particles or when the particle density is unknown (Geller et al. 2006; Park et al. 2004) or varies during a certain process.

A combination of a differential mobility analyzer (DMA) and an APM is often used to measure mass of the mobility classified particles. The particles are classified in a narrow mobility size bin determined by the DMA transfer function (Knutson and Whitby 1975). This spread in the particle diameter leads to a larger spread in particle mass. Thus the trend in particle concentration measured as a function of APM voltage is wider than the APM transfer function even though the particles can be considered as "mono-disperse" in size (Lall, et al. 2008).

A detailed model for inverting the output of the DMA-APM system to determine the input size distribution was previously developed by Emery (2005). Their analysis was analogous to the analysis of Tandem-DMA (DMA-DMA) response function (Rader and Mcmurry 1986; Stolzenburg and McMurry 2008). In our present study, we start with a mobility distribution with the same shape as the DMA transfer function and then compute the APM response function resulting from the known distribution. The DMA transfer function is a triangular function in terms of electrical mobility and can be approximated as a distorted triangular function in terms of the mobility diameter for narrow distributions. The calculations are compared with measurements made with NIST Standard Reference Materials (SRM®) PSL spheres with 60 and 100 nm nominal diameter, and NIST traceable 300 nm PSL spheres. The measured modal diameter (± uncertainty based on 95% confidence) for these SRM® PSL particles are previously reported as 60.39 nm ± 0.63 nm and 100.7 nm ± 1.0 nm (Mulholland et al. 2006). A key advantage of the SRM particles is that they have the lowest uncertainty—highest accuracy—for the mode diameter of any

particles available. This allows us to assess the accuracy of the mass measurement by the APM.

THEORY

APM Transfer Function

The equations of motion inside an APM neglecting Brownian diffusion are (Ehara et al. 1996):

$$\frac{m}{\tau}\frac{dr}{dt} = m\omega^2 r - \frac{qV}{r \ln\left(\frac{r_2}{r_1}\right)} \qquad [1a]$$

where, m is particle mass, q is the charge on the particle and, τ is the particle relaxation time given as:

$$\tau = \frac{m}{f} = \frac{mC(d_p)}{3\pi\mu d_p} \qquad [1b]$$

where f is the friction factor for a spherical particle with diameter d_p.

$$\frac{dz}{dt} = \upsilon \qquad [2a]$$

where, for laminar parabolic flow

$$\upsilon = \frac{3}{2}\upsilon_0 \left[1 - 4\left(\frac{r - r_c}{r_2 - r_1}\right)^2\right] \qquad [2b]$$

and, for uniform flow,

$$\upsilon = \upsilon_0 \qquad [2c]$$

Particles are classified in the APM according to their mass to charge ratio (specific mass), s_c:

$$s_c = \frac{V}{r_c^2\omega^2 \ln(r_2/r_1)} \qquad [3]$$

where for the device we used, radius of the outer electrode, $r_2 = 5.2$ cm, radius of the inner electrode, $r_1 = 5$ cm, and $r_c = (r_1 + r_2)/2 = 5.1$ cm. The APM voltage and rotational speed are denoted by V and ω. According to Equation (3), particle morphology, size, and orientation play no role in particle classification.

The particle trajectory can be determined by solving Equations (1) and (2). Based on the particle trajectories, the particle flux and total particle concentration at the APM exit can be determined. The ratio of exit to inlet particle flux is referred to as APM transfer function. The analytical solution for APM transfer function for uniform flow through the APM is given by Ehara et al. (1996). The transfer function is a trapezoid such that the height of the transfer function trapezoid is given by:

$$t(s) = e^{-\lambda_c} \qquad [4]$$

and the base width relative to s_c is given by:

$$\frac{\Delta s}{s_c} = \frac{4\delta}{r_c}\coth\left(\frac{\lambda_c}{2}\right) \qquad [5]$$

$$\delta = (r_1 - r_2)/2 \qquad [6]$$

$$\lambda_c = 2\tau\omega^2 L/\upsilon_0 \qquad [7]$$

where, λ_c is the classifier performance parameter, which may be interpreted as the ratio of axial (L/υ_0) and radial traversal times ($1/2\tau\omega^2$). The length of the APM column is denoted by L which for this device is 25 cm.

To obtain the APM transfer function for laminar parabolic flow, Equations (1) and (2) are solved numerically to calculate particle trajectories. For numerical calculations, we define a new variable, $p(V, s, r)$ which is equal to 1 if the particle of specific mass, s, enters the APM annular region at radial position, r, and exits, at voltage V. The value of $p(V, s, r)$ is equal to 0 otherwise. Using this definition, the APM transfer function can be calculated as:

$$\Omega_{APM}(V, s) = \frac{\int_{r_1}^{r_2} p(V, s, r)\upsilon(r)r\,dr}{\int_{r_1}^{r_2} \upsilon(r)r\,dr} = \frac{n_{out}(V, s)ds}{n_{in}(s)ds} \qquad [8a]$$

The quantity $n_{out}(V, s)$ is the radially averaged particle number-mass distribution. It is important to note that the particle flux varies across the annular region of the APM. The quantity $n_{in}(V, s)$ is the number-mass distribution that enters the APM. For $\frac{\delta}{r_c} \langle\langle 1$, Equation (8a) can be approximated as:

$$\Omega_{APM}(V, s) = \frac{\int_{r_1}^{r_2} p(r)\upsilon(r)\,dr}{\int_{r_1}^{r_2} \upsilon(r)\,dr} \qquad [8b]$$

We used the above definition (Equation [8b]) for our calculations.

We verified the numerical solution for uniform flow with the above mentioned analytical solution (Equations [4] and [5]) given by Ehara et al. (1996). The APM transfer function for uniform and laminar flows are plotted in Figure 1. Unlike our case, the shape of the transfer function reported by Hagwood et al. (1995) for parabolic flow was not unimodal. This is because the transfer function used by Hagwood et al. (1995) was based on the ratio of probabilities rather than the ratio of fluxes; that is, the velocity term in Equation (8b) was not included.

Brownian Motion Inside the APM

We investigated the effect of Brownian diffusion on the APM transfer function for the conditions discussed in the article. The following equations are solved numerically using a
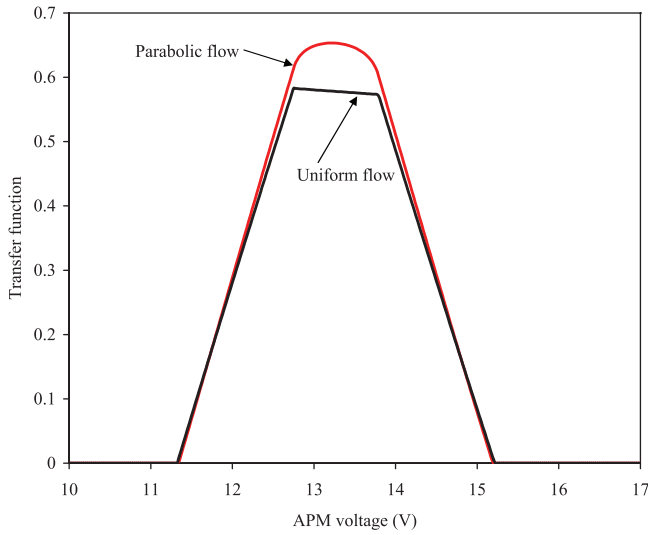
FIG. 1. APM transfer function for uniform and laminar parabolic flow. Particle size: 60 nm. APM rotational speed: 4000 RPM. Flow through the APM = 300 sccm.

Monte-Carlo method.

$$r(t + \Delta) - r(t) = \frac{m\omega^2 r(t)}{(m/\tau)} \cdot \Delta - \frac{1}{(m/\tau)} \frac{qV}{r(t)\ln\left(\frac{r_2}{r_1}\right)} \cdot \Delta$$

$$+ \left(\sqrt{2D\Delta}\right) B_x(t) \qquad [9]$$

$$z(t + \Delta) - z(t) = \upsilon\Delta + (\sqrt{2D\Delta})B_z(t) \qquad [10]$$

where $B_x(t)$ and $B_x(t)$ are Gaussian random variables with zero mean, and standard deviation (or variance) equal to unity. The method was also previously used for both the DMA (Hagwood et al. 1999) and APM transfer functions (Hagwood et al. 1995). Here $p(V, s, r) = 1$ when $z \geq L$ and $r_1 < r < r_2$, and $p(V, s, r) = 0$ when $z \geq L$ and $r \geq r_2$ or $r \leq r_1$.
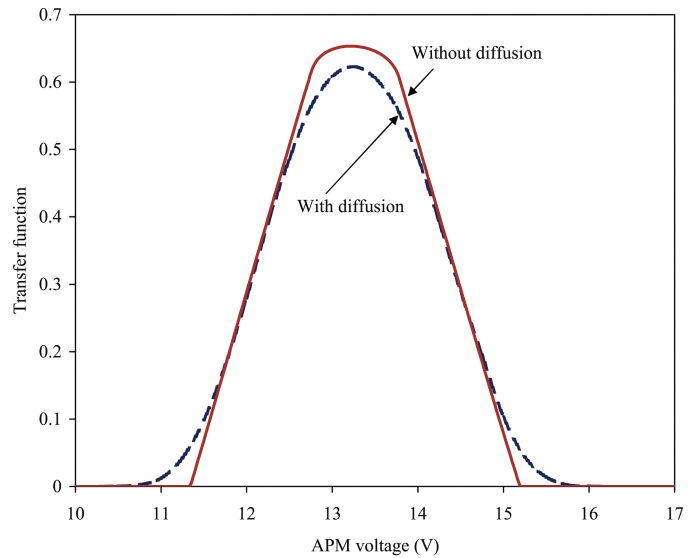
Figure 2a and 2b shows the APM transfer function with uniform flow and laminar parabolic flow respectively, for two cases: Without diffusion (Equations [1] and [2]) and with diffusion (Equations [9] and [10]) for 60 nm PSL spheres. For these calculations, the APM rotational speed was 4000 RPM and the flow through the APM was 300 sccm. Under these conditions, there was only a little broadening of the transfer function due to Brownian diffusion. The difference between the full width at half height (FWHH) of the transfer functions with and without Brownian diffusion is less than 0.5% in Figure 2a. For further analysis in this article, we included the contribution of diffusion broadening on the APM response function.

APM Response Function

We present the following analysis for a narrow triangular particle size distribution (PSD), which nominally represents mo-
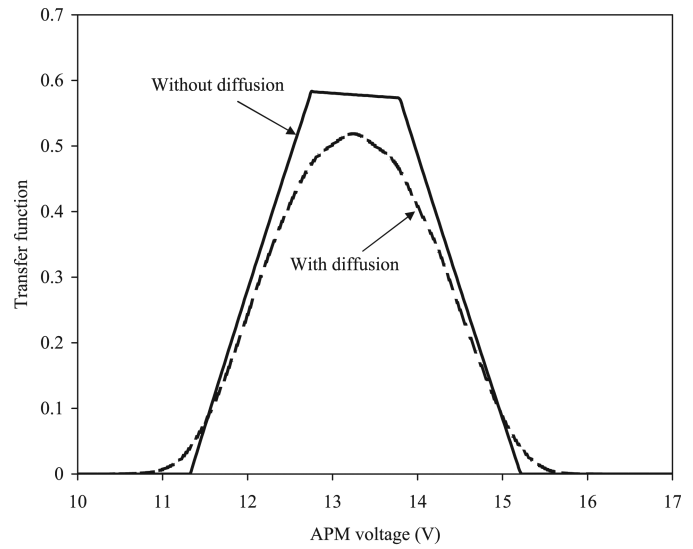
(a)

(b)

FIG. 2. APM transfer function with (a) uniform flow and (b) laminar parabolic flow for two cases: Without diffusion (Equations [1] and [2]) and with diffusion (Equations [9] and [10]). Particle size: 60 nm. APM rotational speed: 4000 RPM. Flow through the APM = 300 sccm.

bility classified particles from a DMA. Figure 3 is a graphical representation of our analysis. The distribution is divided into infinitesimal size bins for which the APM transfer function is calculated. Thus the particles in each bin that exit the APM at a given voltage are determined. The *total* number of particles that exit the APM at a given voltage is the sum over each bin.

Let $G(d_p)$ be a triangular function, which approximately resembles the DMA transfer function, such that it can be used to describe the PSD of particles exiting the DMA. Thus, the exit particle number concentration, dN, in the diameter range d_p to
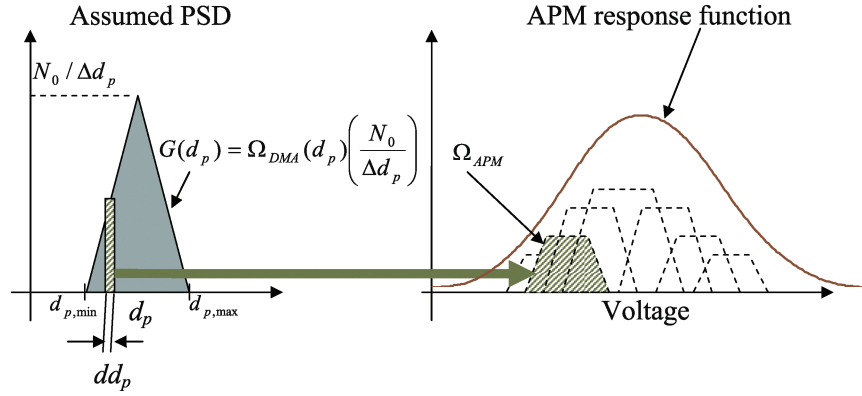
FIG. 3.   Schematic diagram of calculation of APM response to triangular spread in particle size similar to the spread in mobility diameter for particles classified by a DMA (figure not to scale).

$d_p + dd_p$ is given by:

$$dN = G(d_p)dd_p \qquad [11a]$$

where,

$$G(d_p) = \Omega_{DMA}(d_p)n(d_p) = \Omega_{DMA}(d_p)\left(\frac{N_0}{\Delta d_p}\right) \qquad [11b]$$

where $n(d_p)$ is the PSD that enters the DMA, and particles are assumed singly charged. For the narrow range of mobility diameter considered in our analysis, we approximated $n(d_p)$ by a constant function, $N_0/\Delta d_p$, where is N_0 the total concentration of singly charged particles that enters the DMA column with diameter in the range Δd_p. Thus the full base width of triangular function $G(d_p)$ is given by:

$$\Delta d_p = d_{p,min} - d_{p,max} \qquad [11c]$$

where, $d_{p,min}$ and $d_{p,max}$ are the minimum and maximum mobility diameter as shown in Figure 3. The function $G(d_p)$ can be replaced by an appropriate PSD function, if the source spread in near-monodispersed particles is other than from a DMA, such as that from the spread in calibration particles. The choice of the triangular function is described later in the paper. The total number of particles exiting the DMA is equal to the area of the triangle.

Following Equation (8), the APM transfer function for particles of mass, s, and at a fixed voltage, V, is given by $\Omega_{APM}(V, s)$

$$\Omega_{APM}(V, s) = \frac{n_{out}(V, s)ds}{n_{in}(s)ds} \qquad [12]$$

If the density is constant and all the particles are spherical, then

$$\Omega_{APM}(V, d_p) = \frac{n_{out}(V, d_p)dd_p}{n_{in}(d_p)dd_p} \qquad [13]$$

where

$$s = \frac{\rho}{q}\frac{\pi d_p^3}{6} \qquad [14]$$

Now, using Equation (10)

$$dN_{out}(V, d_p) = \Omega_{APM}(V, d_p)dN_{in}(d_p) \qquad [15]$$

$$dN_{out}(V, d_p) = \Omega_{APM}(V, d_p) \cdot \Omega_{DMA}(d_p)\left(\frac{N_0}{\Delta d_p}\right)dd_p \qquad [16]$$

The total number concentration of particles that exit at a given APM voltage is given by:

$$N_{out}(V) = \left(\frac{N_0}{\Delta d_p}\right)\int_{d_{p,min}}^{d_{p,max}} \Omega_{APM}(V, d_p) \cdot \Omega_{DMA}(d_p)dd_p \qquad [17]$$

Equation (17) is similar to Emery's (2005) expression for the convolution of the DMA and APM transfer functions.

EXPERIMENTAL SYSTEM

The PSL particle aerosol was generated using an electrospray (TSI model 3480) or an atomizer built earlier in our laboratory. Suspensions of standard PSL particles (NIST Standard Reference Material, 100 nm and 60 nm were electrosprayed and, NIST traceable 300 nm were atomized; nominal density is 1.05 g/cm^3) were used. Nitrogen was used as a carrier gas at a flow of about 1.5 LPM for both the atomizer, and electrospray. For the atomizer experiments, the aerosol flow was passed through a 1 m long copper tube heated to 70°C, and then through two diffusion dryers (length 30 cm each) placed in series. The heating enhanced the effectiveness of the diffusion dryer in evaporating the water from the droplets containing the PSL spheres.

The PSL particles were size selected using a DMA (TSI model 3081) with a sheath flow of air at 3–5 LPM, and an

TABLE 1
APM parameters used in this study and calculated nominal peak voltages. The flow through the APM was 300 sccm

Nominal diameter (nm)	Rotational speed (RPM)	Peak voltage (Eq. 3) (volts)	λ_c (Eq. 7)
60	4000	13.27	0.548
100	3000	34.55	0.574
300	2000	414.6	1.249

aerosol flow rate of 0.3 LPM. The excess flow from the atomizer or electrospray was sent to a HEPA filter, while the monodisperse flow from the DMA was sent to the APM (Kanomax model APM-10). The output of the APM was measured with a condensation particle counter (TSI 3775 CPC) at the 0.3 LPM low flow mode. The APM was operated at rotation speeds of 2000–4000 RPM. The corresponding values of APM operating parameters are given in Table 1.

RESULTS AND DISCUSSION

We measured the particle size distribution of the PSL particles using a DMA. The mode mobility diameter for 60 nm and 100 nm particles was 63.06 nm and 105.5 nm, respectively. The mode was determined by fitting a log-normal curve in the measured size distribution, and averaging over three number distribution modes. Then the DMA was set to a fixed voltage corresponding to the average mode in number distribu-

tion. This ensured that the mass measurements are made with a mode in number distribution, which corresponds to the NIST SRM® modal diameters. The measurements are reported in Table 2.

Next we tested our method for calculating the APM response function for a narrow spread in particle size. An important step in our calculation is the choice of the narrow PSD that enters the APM. We considered two possible sources for the narrow PSD: (a) DMA transfer function (Ω_{DMA}), and (b) the spread in calibration particle size, $G(d_p)$.

Experiments were conducted for three specific cases as outlined below.

Case 1: Mobility Half-Width Smaller than Spread in Particle Size

The DMA aerosol inlet flow was set to 0.3 lpm and the DMA sheath flow was set to 5 lpm. For these aerosol and sheath flows, the electrical mobility half-width (ΔZ_p) calculated from the DMA transfer function (Knutson and Whitby 1975) is 6%. The mobility diameter and resulting PSD can be calculated from the electrical mobility as follows:

$$\frac{\Delta Z_p}{Z_p} = \frac{\Delta \left(d_p / C(d_p) \right)}{d_p / C(d_p)} = 0.06 \quad [18]$$

where, Z_p is the particle electrical mobility diameter (Friedlander 2000). From Equation (18), the base vertices of $G(d_p)$ were 57.39 and 61.28 nm for 59.36 nm PSL spheres (corresponding

TABLE 2
The mass and diameter of 100 and 60 nm SRM® PSL particles measured using a combined DMA and APM system (measurements 1, 2, and 3). The particles were first classified by the mode mobility diameter using a DMA. Then the mass of the mobility classified particle is measured using an APM. The experiment was repeated three times to estimate the repeatability uncertainty. The average diameter and mass are reported

| Measurement | 100.7 nm PSL spheres | | 60.39 nm PSL spheres | |
	Diameter (nm)	Mass ($\times 10^{-19}$ kg)[†]	Diameter (nm)	Mass ($\times 10^{-19}$ kg)[†]
1	101.29	5.710	59.36	1.149
2	101.27	5.707	59.07	1.132
3	100.96	5.656	59.26	1.143
Average	101.2	5.69	59.23	1.142
Standard deviation	0.18	0.030	0.14	0.0086
u_r^R	—	0.0030 (dimensionless)	—	0.0043 (dimensionless)
SRM size	100.7	5.61	60.39	1.210
Error[††] (%)	+0.5 (dimensionless)	+1.4 (dimensionless)	−1.9 (dimensionless)	−5.6 (dimensionless)

[†]Unit of ($\times 10^{-19}$ kg) not applicable to uncertainty and error.

[††]Error = (Measured diameter – SRM diameter) $\times$ 100/(SRM diameter).

to experiment 1 listed in Table 2 for 60 nm nominal diameter PSL spheres). The value of $G(d_p)$ is set to 1 at 59.36 nm. As an estimate for the standard deviation of the triangular function, we consider an isosceles triangular function with total base width equal to 3.89 nm ($= 61.28 - 57.39$); for this function the standard deviation is equal to $3.89/(2\sqrt{6}) \sim 0.8$ nm.

The standard deviation of the PSD for SRM® 1964 60 nm PSL spheres is 4.9 nm near the peak, with the standard deviation of the entire distribution, 7.9 nm. The comparison of standard deviation of $G(d_p)$ and spread in calibration particle diameter, shows that the chosen triangular function is much narrower than the spread in particle size.

Case 2: Mobility Half-Width Comparable to Spread in Particle Size

For this study, we used SRM® 1963 PSL spheres with a mean size of 100.7 nm (± 1.0 nm uncertainty) and an estimated standard deviation in the PSD of 2.0 nm. As in case 1, the base vertices of $G(d_p)$ were 97.40 and 104.45 for 100.96 PSL spheres (corresponding to experiment 3 listed in Table 2 for 100 nm nominal diameter PSL spheres). The value of $G(d_p)$ is set to 1 at 100.96 nm. As an estimate for the standard deviation of the triangular function, we consider an isosceles triangular function with total base width equal to 7.05 nm ($=104.45 - 97.40$); for this function the standard deviation is equal to $7.05/(2\sqrt{6}) \sim$ 1.4 nm.

The standard deviation of the PSD is 2.0 nm for SRM® 1963 100 nm PSL spheres. The standard deviation of $G(d_p)$ is smaller but comparable to the spread in the calibration particle diameter.

Case 3: Mobility Half-Width Larger than Spread in Particle Size

We also carried out experiments where the mobility half-width is much larger than the spread in the calibration particles. In such a case, the size distribution of particles exiting the DMA is given by the original calibration size distribution rather than the DMA transfer function. Thus, unlike the above two cases, we used the spread in calibration particles to represent the base width of the triangular function (G(d_p), Equation [11b]).

We used NIST traceable PSL particles with mode diameter of 300 nm (± 5 nm uncertainty), and with a standard deviation of 4.2 nm (1.4% of mode diameter, coefficient of variance). For these experiments, the DMA aerosol inlet flow was 0.3 lpm and the DMA sheath flow was 3 lpm. Thus the mobility half-width based on the DMA transfer function is about 10%, and approximately 22 nm in diameter. If we choose the triangular function with half-width of 22 nm, then the standard deviation in the triangular function is equal to ($\sim 22/\sqrt{6}$) = 9 nm. This is large compared to the spread in the original 300 nm PSL spheres (4.2 nm standard deviation). Thus for these calculations, we chose the half width of the total base as 3% of the measured diameter, which corresponds closely to the width based on standard deviation reported for 300 nm particles.

The distribution of calibration particles is sometimes represented by a normal distribution. Thus we additionally investigated the effect of choosing a normal distribution in place of the triangular function. We found no significant difference (based on shape and FWHH) between the effects of the two distributions on the APM response function. In both of these cases, the APM response function depended on the standard deviation of the distribution.

Mass Measurement

To measure the mass of the mode classified particles, we measured the particle concentration downstream of the APM as a function of APM voltage. The number concentration as a function of APM voltages are plotted in Figure 4. Each data point is the average value of over at least 60 number concentration readings where each reading corresponds to a measurement interval of one second. Each measurement with 60 and 100 nm PSL spheres is repeated three times to estimate the repeatability. The measured masses and diameters are given in Table 2.

The average measured mass (Equation [3]) was 1.142×10^{-19} kg and 5.69×10^{-19} kg for 60 and 100 nm PSL, respectively. The difference between measurements and calculated mass, and the mass (Equation [14]) calculated from the NIST standard diameter was –5.7% and +1.4% for 60 nm and 100 nm PSL particles, respectively. The average diameter calculated from APM mass measurements was 59.23 and 101.2 nm, for 60 nm and 100 nm PSL particles, respectively. The difference between APM measured diameters and NIST standard diameter is –1.9% and +0.5% for 60 nm and 100 nm PSL particles, respectively. The average size based on these measurements is within 1 standard deviation of uncertainty in the certified size for SRM 100 nm particles and within about 4 standard deviations of uncertainty for SRM 60 nm particles. The larger difference for 60 nm particles can be attributed to the broader original size distribution, and to the uncertainty in the APM operating conditions, not discussed herewith. Still an agreement within 2% helps to establish the APM as a quantitative instrument for particle mass measurements for at least near-monodisperse spherical particles.

For 300 nm NIST traceable PSL particles, the measured mass, $m_0 = 1.566 \times 10^{-17}$ kg which corresponds to diameter, $d_m = 305.5$ nm for PSL particles (density = 1.05 g/cc). Thus if the PSL nominal size of 300 nm is assumed to be the true size, then the difference in APM measurement is about [(305.5–300)/300] 1.8% in diameter, and 5.6% in mass.

The relative standard uncertainty for the mean mass for repeat measurements, $u_r^R(\bar{m})$, is estimated as the standard deviation of the mean divided by the mean.

$$u_r^R = \left[\frac{\sum_i (m_i - \bar{m})^2}{N(N-1)} \right]^{1/2} / \bar{m}, \qquad [19]$$
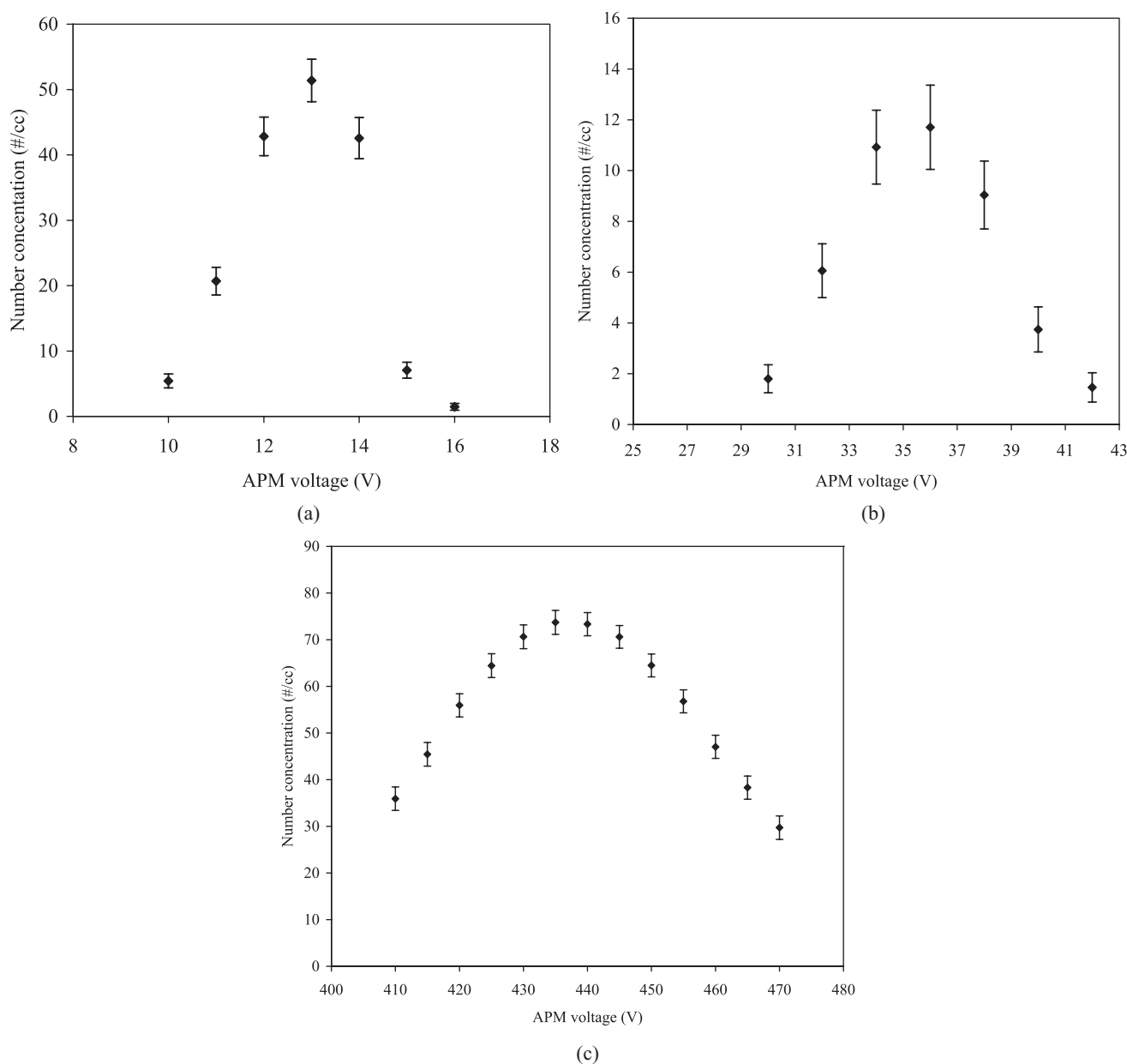
FIG. 4. Particle concentration (particles/cc) measured at different APM voltage for PSL particles with nominal diameter (a) 60 nm, (b) 100 nm, and (c) 300 nm. The APM was operated at 4000, 3000, and 2000 rpm for 60, 100, and 300 nm PSL particles, respectively. Each data point is the average value of over 60 readings; the error bars represent the standard deviation ($\pm\sigma$). The peak of the normal distribution is determined by fitting a normal distribution.

where N is the number of repeat measurements. The experimental data is reported in Table 2. For 60 nm and 100 PSL particles, the repeatability uncertainty in mass measurement was 0.0043 and 0.0031, respectively.

APM Response Function: Comparison of Theory and Measurements

Figure 5 shows a comparison of the calculated and measured APM response function for an initial particle size distribution that enters the APM. The calculations are shown for a triangular PSD described in the previous section. The measured data points are particle concentration measured at different APM voltage. The comparison is shown for PSL particles with nominal diameter equal to (a) 60 nm, (b) 100 nm, and (c) 300 nm. The theoretical curves and measured data points are normalized such that the peak heights are equal. The normalization is done to visually compare the widths of the distribution.

As evident from Figure 5, the calculated APM response function and measured data followed a similar trend with respect to
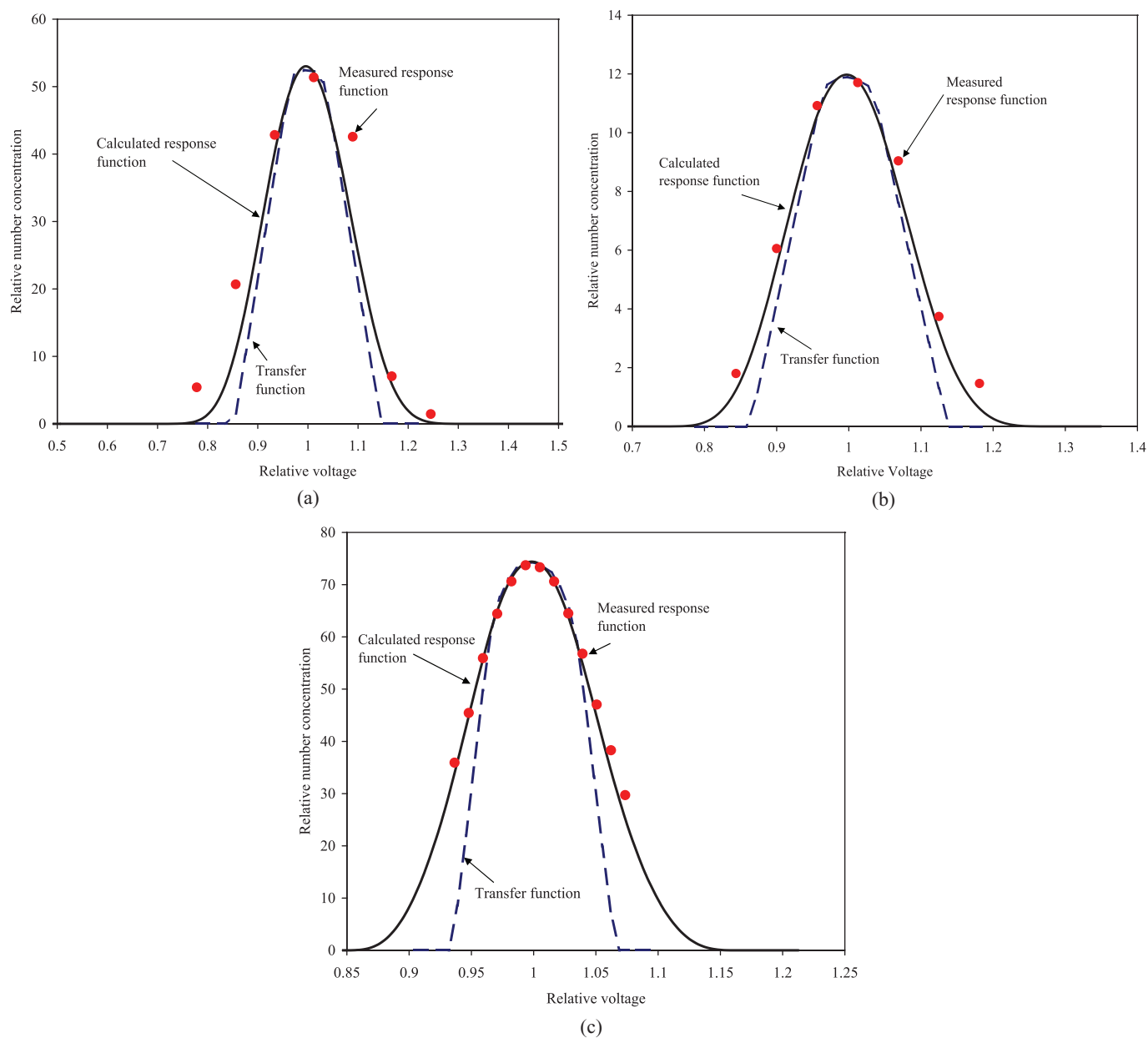
FIG. 5.   Comparison of theoretical and measured APM response functions (Equation [17] with laminar parabolic flow, Equation [2b]) for an initial particle size distribution that enters the APM. The effect of Brownian diffusion broadening is included. The theoretical transfer function without diffusion is also shown for comparison. The measured data points are particle concentration measured at different APM voltage for PSL particles with nominal diameter (a) 60 nm, (b) 100 nm, and (c) 300 nm. The theoretical curves and measured data points are normalized such that the peak heights are equal. The normalization is done to visually compare the widths of the distribution.

APM voltage. However, the theoretical APM transfer function is narrower than the measured APM response.

The comparison of heights of measured data and theoretical APM responses cannot be made because of diffusion losses and other transport losses inside the APM and during transport to the particle counter. As an example, the height of measured data peak was about 40% lower than the calculated APM response function for 300 nm shown in Figure 5c.

CONCLUSIONS

We validate APM mass measurements with calibration PSL spheres of 60, 100, and 300 nm nominal diameter. For all the three sizes, there was agreement within 2% between modal diameter measured by combined DMA-APM system and the modal diameter reported previously for calibration PSL particles.

A method to account for the narrow spread in particle size (near-monodispersed) is suggested. The spread in particle size

can occur due to spread in calibration particle sizes or due to the transfer function of an instrument such as a DMA. The narrow spread in particle size leads to larger spread in particle mass.

We present a simple calculation for a narrow triangular PSD, similar to that of a DMA transfer function. The spread in calibration particle size and spread due to DMA transfer function are considered using three cases: (a) mobility diameter half-width smaller than spread in calibration particle size, (b) mobility diameter half-width comparable to the spread in calibration particle size, and (c) mobility diameter half-width larger than spread in calibration particle size. For all the three cases, there was good agreement in the measured and calculated DMA-APM response function.

We conclude that the narrow spread in the calibration particle sizes and the DMA transfer function should be accounted for in combined DMA-APM measurements.

REFERENCES

Ehara, K., Hagwood, C., and Coakley, K. J. (1996). Novel Method to Classify Aerosol Particles According to Their Mass-to-Charge Ratio—Aerosol Particle Mass Analyser, *J. Aerosol Sci.* 27(2):217–234.

Emery, M. (2005). Theoretical Analysis of Data from DMA-APM System, *Masters Thesis. University of Minnesota.*

Friedlander, S. K. (2000). *Smoke, Dust, and Haze: Fundamentals of Aerosol Dynamics.* Oxford University Press, New York.

Geller, M., Biswas, S., and Sioutas, C. (2006). Determination of Particle Effective Density in Urban Environments with a Differential Mobility Analyzer and Aerosol Particle Mass Analyzer, *Aerosol Sci. Technol.* 40(9):709–723.

Hagwood, C., Coakley, K., Negiz, A., and Ehara, K. (1995). Stochastic Modeling of a New Spectrometer, *Aerosol Sci. Technol.* 23(4):611–627.

Hagwood, C., Sivathanu, Y., and Mulholland, G. (1999). The DMA Transfer Function with Brownian Motion a Trajectory/Monte-Carlo Approach, *Aerosol Sci. Technol.* 30(1):40–61.

Knutson, E. O., and Whitby, K. T. (1975). Accurate Measurement of Aerosol Electric Mobility Moments, *J. Aerosol Sci.* 6:453–460.

Lall, A. A., Rong, W., Madler, L., and Friedlander, S. K. (2008). Nanoparticle Aggregate Volume Determination by Electrical Mobility Analysis: Test of Idealized Aggregate Theory Using Aerosol Particle Mass Analyzer Measurements, *J. Aerosol Sci.* 39:403–417.

McMurry, P. H., Wang, X., Park, K., and Ehara, K. (2002). The Relationship Between Mass and Mobility for Atmospheric Particles: A New Technique for Measuring Particle Density, *Aerosol Sci. Technol.* 36(2):227–238.

Mulholland, G. W., Donnelly, M. K., Hagwood, C. R., Kukuck, S. R., Hackley, V. A., and Pui, D. Y. H. (2006). Measurement of 100 nm and 60 nm Particle Standards by Differential Mobility Analysis, *J. Res. of the National Institute of Standards Technol.* 111(4):257–312.

Park, K., Kittelson, D. B., Zachariah, M. R., and McMurry, P. H. (2004). Measurement of Inherent Material Density of Nanoparticle Agglomerates, *J. Nanoparticle Res.* 6(2–3):267–272.

Rader, D. J., and McMurry, P. H. (1986). Application of the Tandem Differential Mobility Analyzer to Studies of Droplet Growth or Evaporation, *J. Aerosol Sci.* 17(5):771–787.

Stolzenburg, M. R., and McMurry, P. H. (2008). Equations Governing Single and Tandem DMA Configurations and a New Lognormal Approximation to the Transfer Function, *Aerosol Sci. Technol.* 42(6):421–432.

Zhou, L., Rai, A., Piekiel, N., Ma, X., and Zachariah, M. (2008). Ion-Mobility Spectrometry of Nickel Nanoparticle Oxidation Kinetics: Application to Energetic Materials, *J. Phys. Chem. C*, 112(42):16209–16218.